SUPPLEMENTARY INFORMATION

Shape induced symmetry in self-assembled mesocrystals of iron oxide nanocubes

S. Disch et al.

1 Synthesis of nanoparticles

The particles were prepared by thermal decomposition of an iron(III) oleate [R1]. Briefly, 36.5 g sodium oleate (~120 mmol, Sigma-Aldrich, 82 %) and 10.8 g $FeCl_3 \cdot 6H_2O$ (40 mmol, Sigma-Aldrich, 97 %) were dissolved in 140 mL n-hexane, 80 mL ethanol and 60 mL deionized H_2O. The mixture was refluxed for 4 h, the organic phase was separated and washed with deionized H_2O, and the solvent was removed on a rotary evaporator. The iron oleate was dissolved in 200 mL 1-octadecene (Sigma-Aldrich, 90%) and subjected to a vacuum for 90 min at 120 °C. The mixture was transferred to a 1 L three-necked round bottom flask equipped with a Dean-Stark condenser to which 5.7 g oleic acid (20 mmol, Sigma-Aldrich, 90%) were added. Truncated maghemite nanocubes were produced by slowly heating the solution to 320 °C at 2.6 °C min^{-1} where the mixture was refluxed for 30 minutes, prior to a rapid cool down. A small portion of the reaction product was later purified into a black paste after several dilution/flocculation cycles using the solvent/non-solvent pair n-hexane/ethanol. Decantation of the supernatant was aided by using a magnet. The particle concentration in the toluene dispersions was estimated from the solids contents of the paste as determined from TGA experiments in air (39 *wt*%).

We find that the nanocrystals synthesized under gentle reflux conditions (i.e., use of a Dean-Stark condenser) always consist of truncated cubes provided that the experimental conditions (i.e. heating rate, surfactant/precursor molar ratio) defined above are maintained within relatively narrow boundaries. Preliminary studies have also indicated that the ration of sodium oleate to oleic acid influences the faceting and thus the degree of truncation of the nanocubes [R2]. This will be the subject of future studies.

2 Morphological analysis

2.1 Edge length distribution

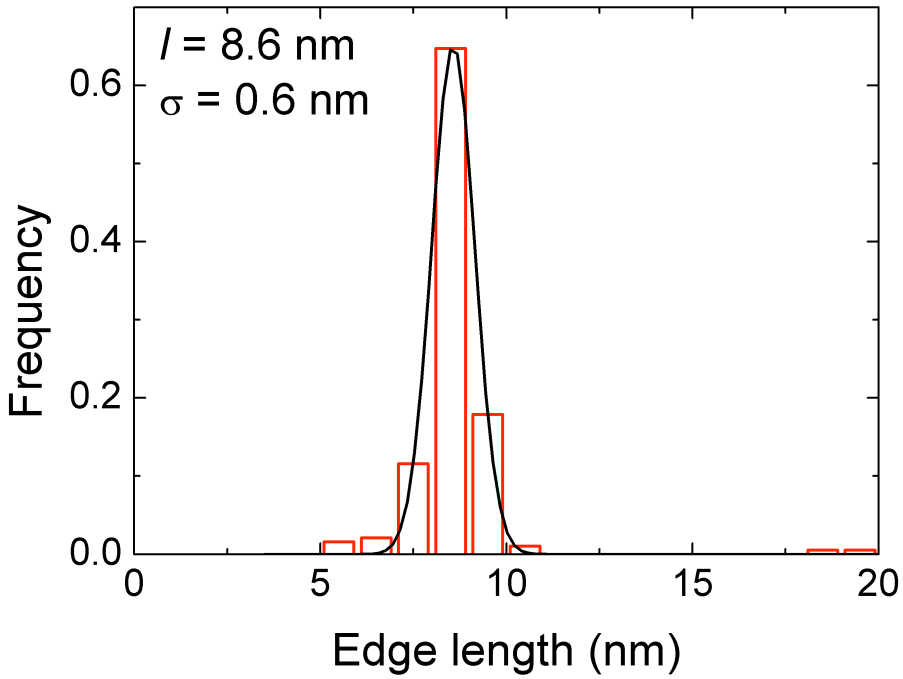

Figure S1: Histograms of the edge length of the cubic nanoparticles. The data is fitted to a Gaussian function.

Transmission electron microscopy (TEM) images and selected area electron diffraction (SAED) patterns of the nanocrystals were obtained using a JEOL JEM-2000 FX microscope equipped with a LaB_6 filament operated at 200 kV (Cs = 3.4 mm, point resolution = 0.31 nm). The specimens were prepared by depositing 2 µL of a toluene dispersion of nanoparticles ($C \sim 10^{14}$ particles/mL) on carbon-coated copper grids and the solvent was allowed to evaporate rapidly. The images were recorded with a CCD camera (Keen View, SIS analysis, 1376×1032 px^2, pixel size 23.5×23.5 μm^2) at 100 k× magnification. High resolution TEM (HRTEM) images of the above-mentioned specimens were obtained using a JEOL JEM-3010 microscope equipped with a LaB_6 filament operated at 300 kV (Cs = 0.6 mm, Cc = 1.3 mm, point resolution = 0.17 nm) and a CCD camera (KeenView, SIS analysis, 1376×1032 px^2, pixel size 6.45×6.45 μm^2) at 800 k× magnification. The edge length, l_i, was manually determined of at least 200-300 nanocubes from the TEM micrographs. The mean cube edge length, l, and its standard deviation, σ, were determined by fitting the corresponding histogram (Figure S1) with a Gaussian distribution function:

$$f(x) = -\frac{1}{\sigma\sqrt{2\pi}}\exp\left[-\frac{(x_i - x_c)^2}{2\sigma^2}\right] \qquad (1)$$

The statistical analysis gives in an edge length, $l = 8.6 \pm 0.6$ nm.

2.2 Small angle X-ray scattering (SAXS)

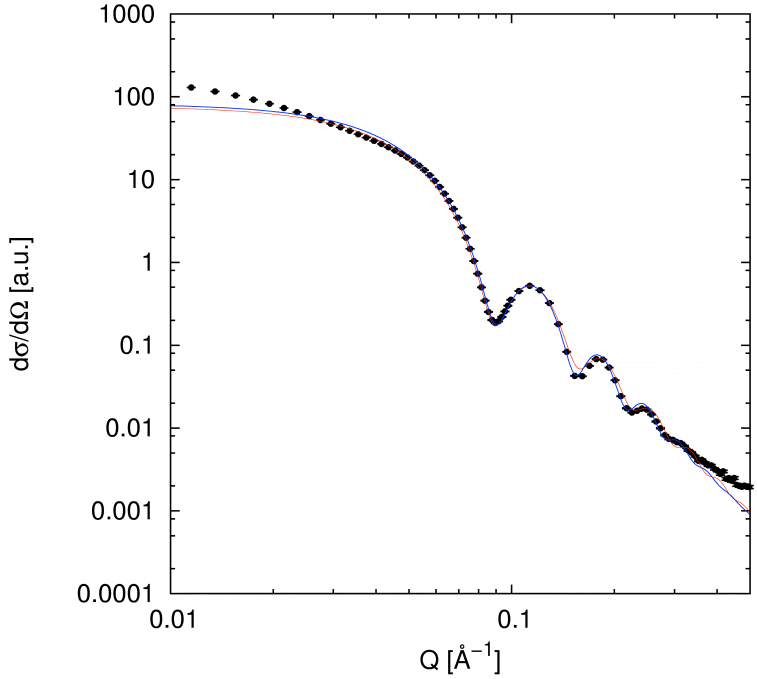

Figure S2: SAXS of iron oxide nanocubes dispersed in toluene. Refinements using a spherical (blue line) and a truncated cubic (red line) form factor are shown.

The small angle X-ray scattering (SAXS) data of dispersed iron oxide nanocubes measured at the JUSIFA beamline at HASYLAB, DESY, Germany, is shown in Figure S3. Data have been fitted using the expressions for (a) a spherical form factor and (b) a truncated cubic form factor. Particles with a diameter of 10.12(1) nm and a lognormal size distribution of 6.6(1) % were obtained using the spherical form factor. Truncated cubes with an edge length l_{SAXS} = 8.5(1) nm and a lognormal size distribution of 6 % were obtained through the cubic form factor.

3 Structural characterization

3.1 Selected area electron diffraction

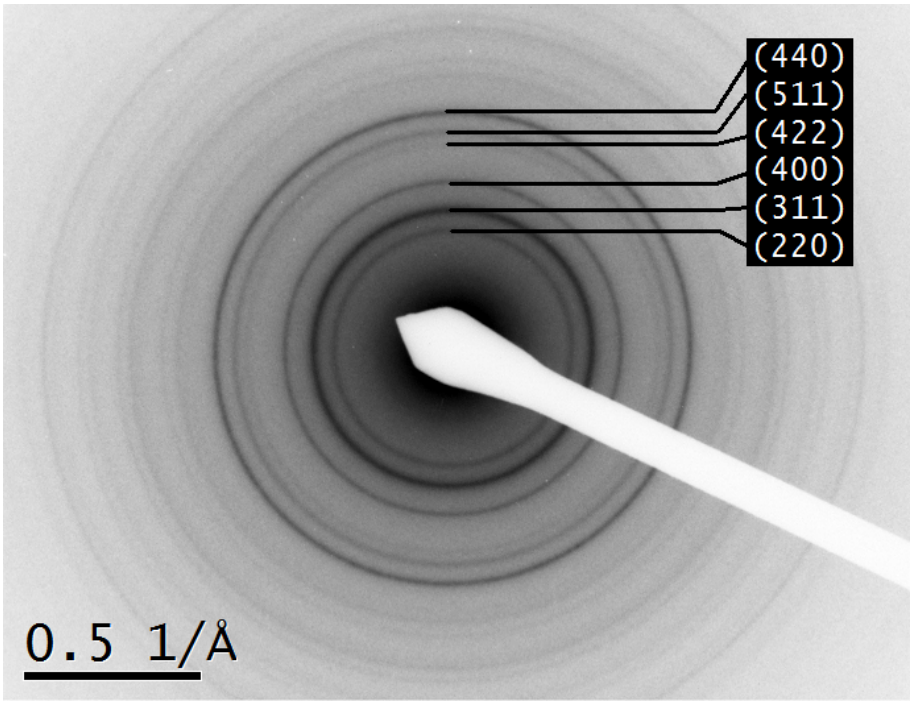

Figure S3: Selected area electron diffraction patterns of the nanocubes taken from a collection of randomly oriented nanoparticles. The first six reflections are indexed to the inverse spinel structure (JCPDS Card # 19-0629)

4 Magnetic measurements

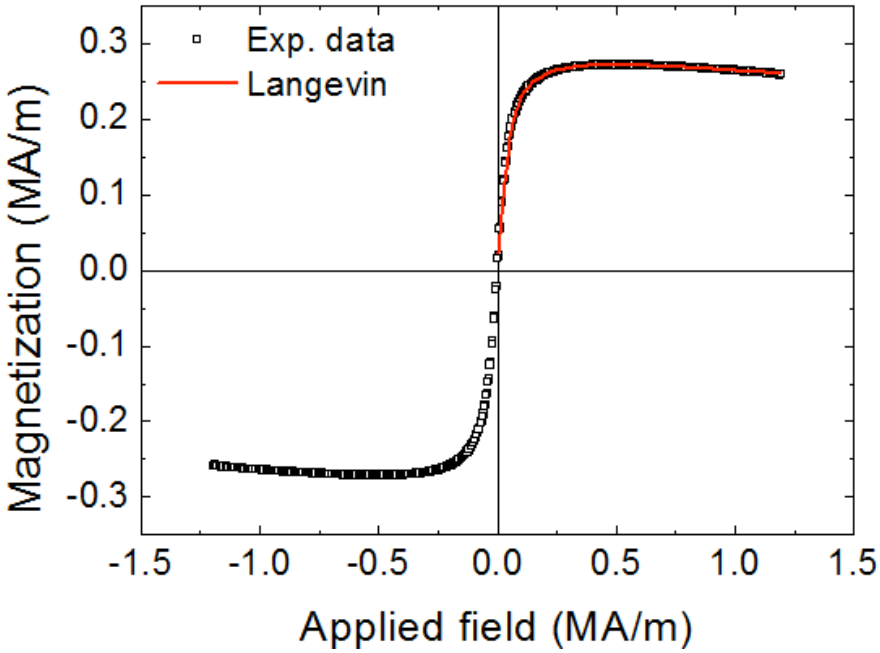

Figure S4: Magnetization versus applied field curves for the iron oxide nanocubes at room temperature. The open symbols and the lines correspond to the experimental data points and the fitting with Langevin's equation, respectively.

Magnetic measurements using a Quantum Designs Physical Property Measuring System (PPMS-9) equipped with a superconducting magnet and a vibrating sample magnetometer (VSM) option, were carried out on a small amount (ca. 10 mg) of a paraffin dispersion with a concentration of ca. 0.1 *wt.*% of the iron oxide nanocubes. The M-H curves were measured using a maximum field $\mu_0 H$ = 1.5 T (1.2 MA/m = 15 kOe). The demagnetizing portion was fitted with the Langevin equation, i.e., $M = M_S\left[\coth(mH/kT) - (kT/mH)\right] + \chi H$. $m = \mu_0 M_S V_{mag}$, μ_0 is the permeability in vacuum ($\mu_0 = 4\cdot10^{-7}$ Tm/A), V_{mag} corresponds to the volume of the particle, M_S is the saturation magnetization, k is Boltzmann's constant, T the temperature, M the magnetization, χ the susceptibility at high fields, and H the applied field. A particle volume of V_{mag} = 495 nm^3 was thus obtained for the cubes. These values would correspond to ideal cubes with an edge length l_{mag} = 7.9 nm. The saturation magnetization of the sample was found to be 59.6 emu/g.

5 Interparticle energies

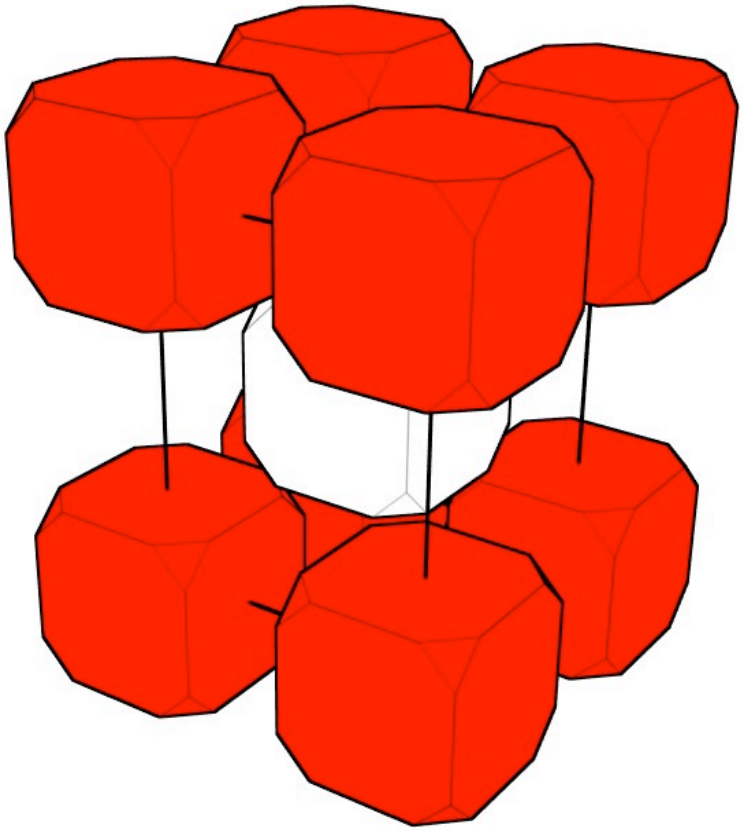

Figure S5: 3D view of the bct unit cell, with a=13.10(5) nm and c=17.8(5) nm.

The attractive interparticle van der Waals (*vdW*) energy for a reference particle in a given array can be estimated at first approximation by summation of the interaction potentials exerted on a particle by its first- (*fnn*), second- (*snn*), and third nearest neighbours (*tnn*). The magnitude of the interparticle *vdW* energy is dependent not only on the size and distance between the objects but also on their shape. Hence, the inherent anisotropic morphology of the nanocubes and the body-centered tetragonal (*bct)* structure requires different geometrical models to be used in order to account for this anisotropy (see Figure S6). There are three basic types of interactions to consider; face-face, edge-edge, and corner-corner. Table 1 illustrates the number of neighbours and their type of type for a reference particle in a *bct* lattice as well as a hypothetical simple cubic (*sc*) lattice. Note that particles at distances $h > l$ are not considered.

The interparticle distances are readily obtained considering the dimensions of the *bct* unit cell a=13.1 nm and c=17.8 nm (c/a=1.36) obtained through GISAXS data and the cube's edge length l_{SAXS} = 8.5 nm. Thus, the body diagonal is $L_{bct,111} = \sqrt{2a^2 + c^2} = 25.7$ nm. The portion of the *bct* body diagonal contained within a cube is $p = \frac{l}{\sin\gamma} = 12.3\,\mathrm{nm}$, where γ is the angle between the body diagonal $L_{bct,111}$ and the face diagonal of the basal plane

$L_{bct,110} = \sqrt{2}a$. The experimental interparticle distance, h_0, along t, $L_{bct,111}$, then becomes $h_0 = \frac{1}{2}L_{bct,111} - p = 0.6\,\text{nm}$. In the case of a hypothetical *sc* array, the geometry is simpler and the value for the face-face interparticle distance, h_1^{sc} = 3.8 nm, was obtained by manually measuring the interparticle distances in a square array from TEM images. This distance agrees well with twice the length of the oleic acid molecule and previously reported values for the separation distances[R1a].

The interparticle distances h_1^{sc} and h_2^{sc} in a hypothetic *sc* array are not expected to vary with τ when the array is formed with particles with a degree of truncation in the range $0 < \tau < 0.58$, i.e., ranging between an ideal cube and an Archimedean truncated cube, respectively. However, the interparticle distances in the *bct* array should be strongly dependent on τ. This can be quantified considering that (1) a corner-corner distance $h_0 = 0.6$ nm is the minimum allowable separation distance and (2) the face-face and edge-edge interparticle distances in the basal plane of the tetragonal structure are constant (constant *intralayer* distances h_1 and h_2). We assume a maximum distance between the ABAB layers h_{AB} = 3.8 nm (variable *interlayer* distance), which refer to two times the distance of a dense oleic acid layer. We let h_0 vary linearly with the degree of truncation in the interval $0 < \tau < 0.45$; $h_0 \equiv 0.6$ nm in the interval $0.45 < \tau < 0.58$.

5.1 Face-face and edge-edge interactions

The interparticle attractive energies for two (perfect, non-truncated) cubes with an edge length, l, interacting face-face and edge-edge at a distance h can be calculated using Hamaker-type expressions. These are given by Eqs. (3) and (6), respectively[R4]. The interparticle energy associated with two truncated cubes, should to the first approximation vary with the area of the truncated facet, which in the case of cubic maghemite would correspond to the {100} exposed planes. We find that the facial area diminishes only 10 % as the degree of truncation increases from zero to $\tau = 0.45$. Regarding the edge-edge interactions, the volume of the cube at the distance h_2 at $\tau = 0.45$ decreases only 15 %. Hence, for the sake of simplicity, we have estimated the face-face and interactions assuming perfect, non-truncated cubes.

$$U_{vdW}^{face} = -\frac{A}{\pi^2 kT} K_f(x)\Big|_{h+lh+l}^{h+2lh} \tag{3}$$

where

$$K_f(x)\Big|_{h+lh+l}^{h+2lh} = K_f(h+2l) + K_f(h) - 2K_f(h+l) \tag{4}$$

$$K_f(x) = \frac{1}{4}\ln\left(\frac{x^4 + 2x^2l^2 + l^4}{x^4 + 2x^2l^2}\right) + \left(\frac{x^2 - l^2}{4lx}\right)\arctan\left(\frac{l}{x}\right)$$
$$+ \left(\frac{x^2 - l^2}{4lx}\right)\arctan\left(\frac{l}{x}\right) + \frac{2^{3/2}xl^3}{6l^4}\arctan\left(\frac{1}{\sqrt{2}}\frac{x}{l}\right)$$
$$+ 2l\left(\frac{1}{6x^2} + \frac{1}{6l^2}\right)(x^2 + l^2)^{1/2}\arctan\left[\frac{l}{(x^2 + l^2)^{1/2}}\right] \tag{5}$$

and

$$U_{vdW}^{edge} = -\frac{A}{\pi^2 kT} K_e(x)\Big|_{h+lh+l}^{h+2lh} \tag{6}$$

with

$$K_e(x)\Big|_{h+lh+l}^{h+2lh} = K_e(h+2l) + K_e(h) - 2K_e(h+l) \tag{7}$$

$$K_e(x) = \frac{1}{8}\ln\left(\frac{x^2 + h^2}{l^2 + h^2 + x^2}\right) + \frac{1}{8}\left(\frac{x}{h} - \frac{h}{x}\right)\arctan\left(\frac{h}{x}\right) + \frac{x(l^2 + h^2)^{3/2}}{12l^2h^2}\arctan\left(\frac{x}{(l^2 + h^2)^{1/2}}\right)$$
$$+ \left(\frac{l(h^2 + x^2)^{1/2}}{12}\right)\left(\frac{1}{h^2} + \frac{1}{x^2}\right)\arctan\left(\frac{l}{(h^2 + x^2)^{1/2}}\right)$$
$$+ \left(\frac{h(l^2 + x^2)^{1/2}}{12}\right)\left(\frac{1}{l^2} + \frac{1}{x^2}\right)\arctan\left[\frac{h}{(x^2 + l^2)^{1/2}}\right] \tag{8}$$

where A is the Hamaker constant for iron oxide in hydrocarbon medium ($A = 1.6 \cdot 10^{-20}$ J), k is Boltzmann's constant, T the temperature, and K_f and K_e the pair-wise integration functions for face-face and edge-edge interactions, respectively.

5.2 Corner-to-corner approximation

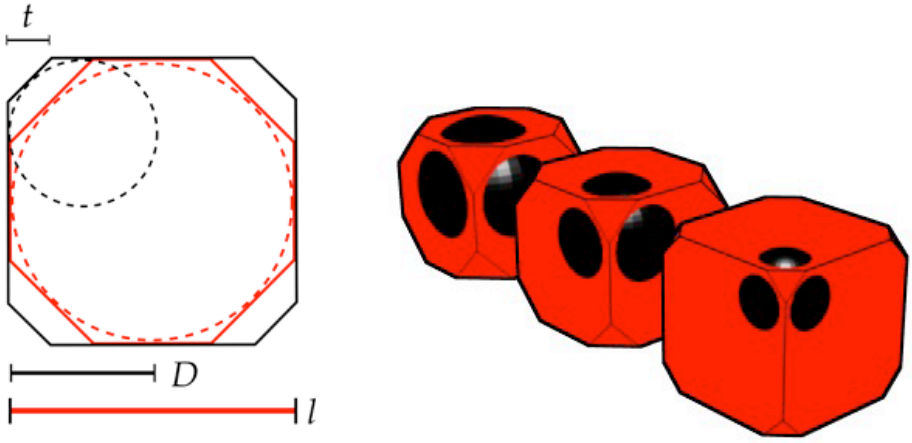

Figure S6. (Left) Illustration of the geometric scaling approximation for diagonally interacting particles. (Right) Truncated cubes with τ=0.58, 0.45 and 0.3 and their corresponding spheres, with diameter* D *used for the approximation of the diagonal interaction energy.

The interaction energy associated with two truncated cubes interacting diagonally should vary with the area of the truncated facet, which in the case of cubic maghemite would correspond to the {111} exposed planes, and the interparticle distance.

We have approximated the corner-corner interaction of two truncated cubes at moderate truncations ($0.3 < \tau < 0.58$) with two spheres. The size of the spheres was determined from the diameter of the circle that touches a minimum of three of the sides of the 2D projection of the cubes, $D = (2+\sqrt{2})t$ (see Figure S7). Translated to 3D, this results in an equivalent sphere, which describes conveniently the interaction volume at short interparticle distances. For an ideal truncated cube (one of the Archimedean solids) it can be shown that $\tau = \frac{\sqrt{2}}{\sqrt{2}+1}$ so that $D \equiv l$. Note that at decreasing truncations ($\tau, t \to 0$) $D \to 0$, i.e., the sphere shrinks to a point, leading to an incremental underestimation of the attractive interparticle energy whereas at large truncations ($\tau > 0.58$), the interacting areas become increasingly large and the interaction would resemble more a face-on interaction.

Hence, at moderate truncations the corner-to-corner interaction can be approximated with the well-know expression for two spheres with equal diameter, D, spaced at a distance h:[R5]

$$U_{vdW}^{sphere} = -\frac{A}{12kT} K_{sp}(h, D) \qquad (9)$$

with

$$K_{sp} = \left[\frac{D^2}{h^2 + 2hD} + \frac{D^2}{(h+D)^2} + 2\ln\left(\frac{h^2 + 2hD}{(h+D)^2} \right) \right] \qquad (10)$$

where K_{sp} is the pair-wise integrated function for two equal spheres.

5.3 Summary

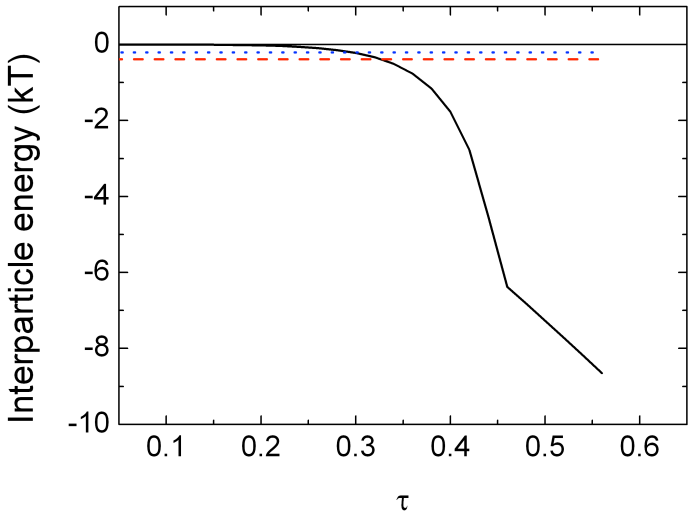

Figure S7: Variation of the corner-to-corner contribution to the interparticle energies as a function of τ for a truncated cube in a* bct *lattice as described in Table S1 (black line). The contributions from face-face (red line), and edge-edge (blue line) interacting ideal cubes are also included.

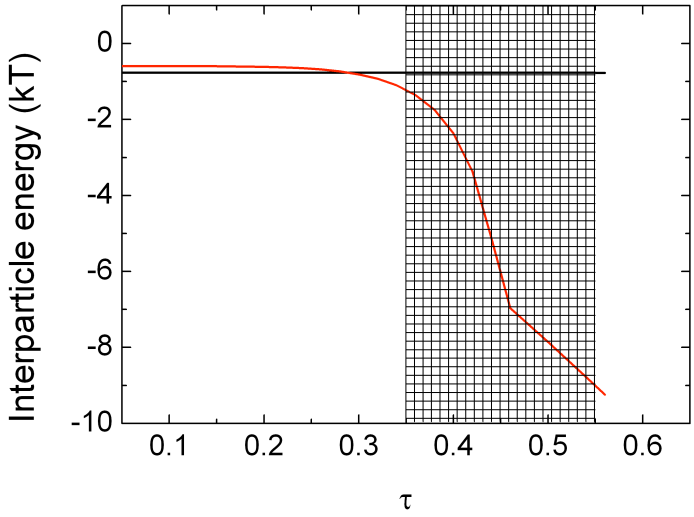

Figure S8: Interaction energies for a truncated cube in* sc *(black) and* bct *(red) lattice. The hatched region indicates the experimental distribution of τ.

The interparticle energies for the *sc* and *bct* lattices have been calculated using Eqs. (3), (6), and (9), and are plotted in Figure S7. The individual contributions of the corner-corner (eight-fold), face-face (four-fold), and edge-edge (four-fold) interactions are shown in Figure S8. The model is based on the assumptions that (1) the face-face and edge-edge interactions in the *bct* (and *sc*) structures do not vary with τ, and (2) that neither the interparticle distance h_1 nor h_2 of the *bct* structure vary with τ. The kink in the curves at $\tau = 0.45$ is a consequence that beyond this degree of truncation, the interparticle distance h_0 is not allowed to decrease to a value smaller than $h_1 = 0.6$ nm. Figure S8 shows how the sum of all contributions to the interparticle energies varies with the degree of truncation, τ, for the *sc* and *bct* lattices. The results indicate that it is the reduced interparticle distance along the diagonals that renders the *bct* structure with a higher stability than the *sc* lattice. This simple model also suggests the formation of a range of structures with decreasing symmetry, such as *sc* → *fcc* → *bct* to a probable body-centered cubic (*bcc*) when the degree of truncation is increased towards a cuboctahedron.

6 Estimation of the magnetic dipole interactions

6.1 Dipole interactions between nanoparticle pairs

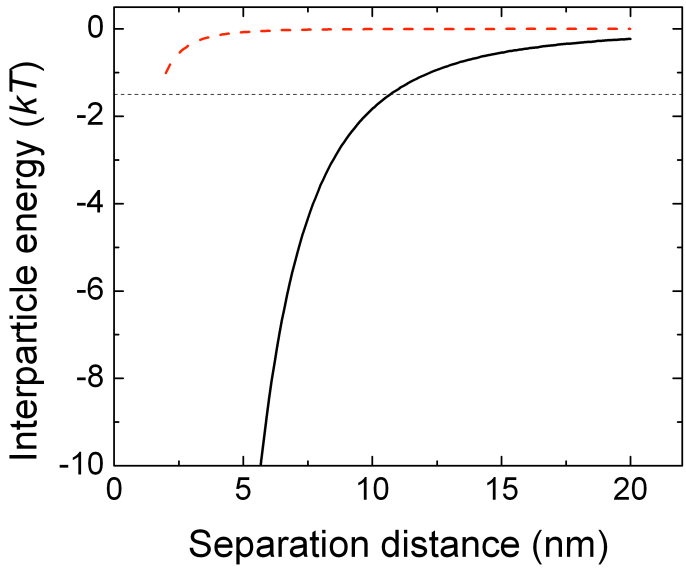

Figure S9:* vdW *(red broken line) and dipolar (black solid line) interparticle energy for a nanocube pair calculated using Eqs. (3) and (11) at various separation distances. The dashed horizontal line indicates 3/2 kT.

The pair-wise magnetic dipolar interaction energy, U_{dip}, can be calculated using an expression for two point dipoles with moments μ_i at a separation distance r as shown in Eq. (11). It must be noted that although the nanoparticles are superparamagnetic at room temperature, the calculations will be performed considering that the nanoparticles do sustain a stable magnetic moment $\mu_1 = \mu_2 = \mu = 2.1 \cdot 10^4\ \mu_B$ (where μ_B corresponds to Bohr's magneton), as determined from the magnetic measurements shown in Fig. S4. This approximation is valid considering that the Zeeman energy, E_{Zeeman}, is sufficiently large under an applied magnetic field of $\mu_0 H = 0.03$ T (see Eq. (12)).

$$U_{dip} = \frac{\mu_0}{4\pi r^3}\left[\vec{\mu}_1\vec{\mu}_2 - \frac{3}{r^2}(\vec{\mu}_1\cdot\vec{r})(\vec{\mu}_2\cdot\vec{r})\right] \tag{11}$$

$$E_{Zeeman} = -\mu\mu_0 H = -5.843\cdot 10^{-21} J \tag{12}$$

Figure S9 shows both the face-face *vdW* and dipolar pair-wise interparticle energy for nanocubes at various separation distances calculated according to Eqs. (3) and (11), respectively, where the magnetic dipolar interactions were estimated assuming a head-to-tail configuration of the dipoles. We find that the magnetic dipolar two-body interaction is significantly stronger than the particle thermal energy (~3/2 *kT*) at separation distances below ~10 nm while the *vdW* pair interaction for the nanocubes is too weak at separation distances

larger than 2 nm to form stable clusters. This suggests that it is the applied magnetic field which promotes the formation of stable clusters or chains of particles aligned along the dipolar axis in solution.

6.2 Dipole interactions within mesocrystals

We have also made an estimation of the (multi-body) magnetic dipole interactions between the particles in a mesocrystal assuming both *bct* and *sc* arrangements using the expression given by Eq. (11). Due to the large Zeeman energy (see Eq. (12)), a ferromagnetic arrangement of all nanoparticle moments perpendicular to the substrate (i.e., parallel to the *c* lattice constant) will be assumed in a first approximation.

For the *bct* arrangement with a = 13.1 nm and c = 17.8 nm, the following nearest neighbor interaction energies are obtained:

face-face: $U_{dip,bct}^{100} = 1.687 \cdot 10^{-21}$ J

$U_{dip,bct}^{001} = -1.345 \cdot 10^{-21}$ J

edge-edge: $U_{dip,bct}^{110} = 5.97 \cdot 10^{-22}$ J

corner-corner: $U_{dip,bct}^{\frac{111}{222}} = -7.87 \cdot 10^{-22}$ J

leading to a magnetic dipole interaction energy of

$$U_{dip,bct} = 4\ U_{dip,bct}^{100} + 2\ U_{dip,bct}^{001} + 4\ U_{dip,bct}^{110} + 8\ U_{dip,bct}^{\frac{111}{222}} = 1.45 \cdot 10^{-22}\ \text{J}$$

For the *sc* arrangement the contributions are:

face-face: $U_{dip,sc}^{100} = 1.687 \cdot 10^{-21}$ J

$U_{dip,sc}^{001} = -3.374 \cdot 10^{-21}$ J

edge-edge: $U_{dip,sc}^{110} = 5.97 \cdot 10^{-22}$ J

$U_{dip,sc}^{101} = -2.98 \cdot 10^{-22}$ J

corner-corner: $U_{dip,sc}^{\frac{111}{222}} = 0$ J

leading to a magnetic dipole interaction energy of

$$U_{dip,sc} = 4\ U_{dip,sc}^{100} + 2\ U_{dip,sc}^{001} + 4\ U_{dip,sc}^{110} + 4\ U_{dip,sc}^{101} + 8\ U_{dip,sc}^{\frac{111}{222}} = 0\ \text{J}$$

The dipole interaction energy for a particle in the *bct* arrangement, $U_{dip,bct}$, tends to diminish with every further coordination shell taken into account whereas the dipole interaction energy for a particle in an *sc* arrangement, $U_{dip,sc}$, tends to cancel out.

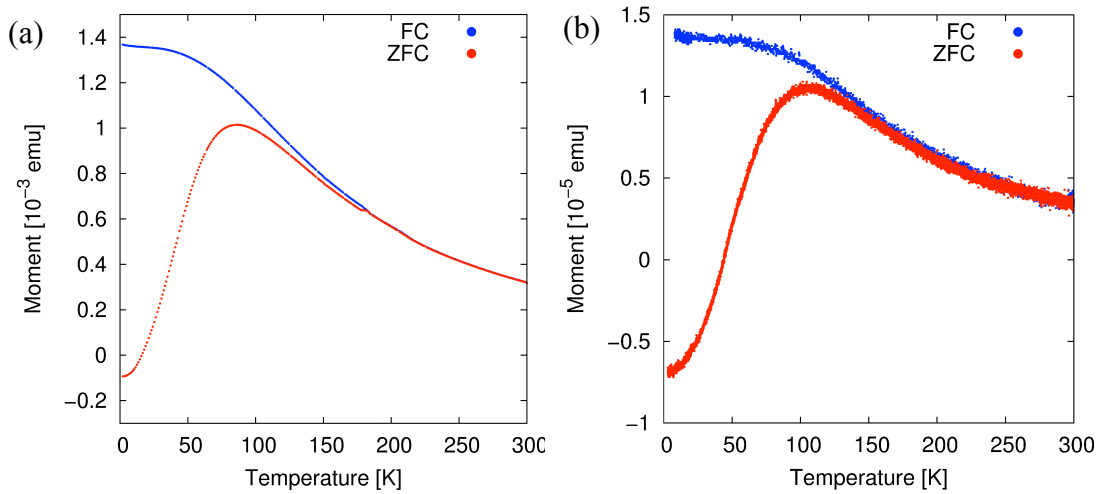

Figure S10: FC/ZFC magnetization measurements of (a) a dilute dispersion of nanocubes and (b) bct ordered nanocubes mesocrystals under and applied field $\mu_0 H$ = 5 mT.

Figure S10 (a) and (b) present field cooled and zero-field cooled magnetization measurements of nanocubes dispersed in toluene and deposited mesocrystals, respectively. The superparamagnetic blocking temperature was determined as T_B = 85 K for the non-interacting dispersion and T_B = 105 K for the deposited mesocrystals. From the difference of the observed blocking temperatures it is possible to estimate the difference in energies of the non-interacting and interacting nanocubes using

$$\Delta E_{mesocrystals} - \Delta E_{dispersion} = \ln\left(\frac{\tau}{\tau_0}\right) \cdot k_B \left(T_{B,mesocrystals} - T_{B,dispersion}\right) = 5.7 \cdot 10^{-21} J \qquad (13)$$

with an attempt frequency of $1/\tau_0 = 10^9$ s^{-1} and a characteristic timescale of τ = 1 s.

The van der Waals interaction energy at room temperature in a body centered tetragonal mesostructure depends on the degree of truncation as shown in Figure S8. We find that for nanocubes with a degree of truncation τ = 0.45(5), the interaction energy per particle is $U_{vdW}(0.45) = -6k_BT = -2.5 \cdot 10^{-20} J$, and even for a degree of truncation of 0.40, we obtain an interaction energy, $U_{vdW}(0.40) = -2.4k_BT \approx -1 \cdot 10^{-20} J$, larger than the dipolar interaction energy.

The calculations show that the magnetic dipolar interactions are more important than the van der Waals interactions to form stable two-particle (or chained) clusters. However, due to the directionality of the dipoles in the mesocrystal, even the largest contribution to the dipole interaction energy, which is the U_{dip}^{001} contribution, is significantly lower than the additive van der Waals interactions. For this reason, the van der Waals interaction energy is considered to be the dominating multi-body interaction in the nanoparticle arrays controlling the preference of the *bct* against the *sc* mesocrystal structure.

References

R1 (a) Ahniyaz, A. and Sakamoto, Y. & Bergström, L. Magnetic field-induced assembly of oriented superlattices from maghemite nanocubes. *Proc. Natl. Acad. Sci. USA* **104,** 17570-17574 (2007). (b) Song, Q. & Zhang, Z. J. Shape control and associated magnetic properties of spinel cobalt ferrite nanocrystals. *J. Am. Chem. Soc.* **126,** 6164–6168 (2004). (c) Salazar-Alvarez, G., *et al.* Cubic versus spherical magnetic nanoparticles: the role of surface anisotropy. *J. Am. Chem. Soc.* **130,** 13234–13239 (2008).

R2 Bodnarchuk, M. I., et al., Large-area ordered superlattices from magnetic wüstite/cobalt ferrite core/shell nanocrystals by doctor blade casting. *ACS Nano* **4**, 423-431 (2010).

R3 Busch, P., Rauscher, M., Smilgies, D.-M., Posselt, D. & Papadakis, C. M. Grazing-incidence small-angle X-ray scattering from thin polymer films with lamellar structures – the scattering cross section in the distorted-wave Born approximation. *J. Appl. Cryst.* **39**, 433-442 (2006).

R4 Parsegian, V.A. *Van der Waals forces: a handbook for biologists, chemists, engineers, and physicists* (Cambridge University, New York, 2006).

R5 Hamaker, H.C. The London-van der Waals attraction between spherical particles. *Physica* **4,** 1058-1072 (1937).